CHAPTER 2

Synthesis and Experimental Optimizations in $(1-x)Ba(Cu_{1/3}Nb_{2/3})O_3-(x)PbTiO_3$ Ceramics

CHAPTER 2.

Synthesis and Experimental Optimizations in (1-x)Ba(Cu$_{1/3}$Nb$_{2/3}$)O$_3$-(x)PbTiO$_3$ Ceramics

2.1   Introduction

In order to investigate the physical characteristics of any solid solution, sample synthesis in phase pure form is essential. As discussed in chapter 1, the formation of pure BCN has not been achieved at the calcination step in well resolved diffraction peaks by earlier researchers in the reported literature till date. To the best of our knowledge synthesis details and XRD pattern of any composition of the (1-x)BCN-(x)PT solid solution hasn't been reported in the literature. As discussed in the subsequent chapters, the crystallographic phase evolution as a function of composition is quite complex for this system. Its synthesis in the pure phase, is therefore, also challenging to obtain in some of the composition ranges. In view of this, typically four different synthesis practices (combinations of milling, calcination and sintering conditions) have been used for the solid solution. The details of the adopted methodology for the synthesis of pure samples for the present work is described in this chapter.

The chapter starts with a brief introduction to the instruments used in synthesizing and characterizing the investigated samples, viz. ball milling, x-ray diffraction (XRD), scanning electron microscopy (SEM), x-ray photoelectron spectroscopy (XPS), P-E loop tracer, Impedance analyzer, d$_{33}$ meter, etc. The details of the Rietveld crystal structure refinement, a software-based crystal structure analysis technique, is covered in

the Section 2.5. The chapter also presents the description of the synthesis process of the solid solution in ceramic form, which is followed by the details of optimization of calcination and sintering conditions for various compositions. Details of the instruments (make, model) used in the present work have also been described at the end of this chapter.

2.2 Brief Introduction of the Instruments used for Synthesis and Characterization of the (1-x)BCN-(x)PT Solid Solution

2.2.1 Ball Mill

A ball mill is a grinder that uses an internal cascade process to homogeneously mix materials such as ores, chemicals, ceramics, and paints. In ball milling, the cylindrical jars spin around an axis with small balls, striking against the wall while spinning [69]. The ratio of the weight of the balls and the material is taken according to the desired mixing extent. The ratio of reactants to balls for (1-x)BCN-(x)PT was kept at 1:10. The mixing jars and the balls are made up of hard materials like zirconia or agate. A solvent, usually ethanol, is partially filled in the grinding media to prevent excessive heating. Intense grinding effects emerge from the ensuing centrifugal and coriolis acceleration [69]. In some cases, the high energy milling for longer duration can result into formation of product phase and the process is termed as mechanochemical synthesis. As a result of the motion and impact of the grinding balls, the powders are subjected to mixing and grinding. A typical high-energy ball mill is shown in Fig 2.31 with a capacity of four jars operating at a maximum of 300rpm in clockwise and anticlockwise directions for desired time durations.

Fig 2.1 A typical Retsch PM400 MA high energy ball mill

2.2.2 Hydraulic Press

To study the bulk characteristics of the materials, one needs dense pellets of the desired material which can be obtained by compact packing of ball milled powders and heating it for densification to occur. The powders can be pressed in a uniaxial hydraulic press by the cold-compaction method. A typical hydraulic press in shown in Fig 2.2. The hydraulic press provides a clamping stage with the ability to exert uniaxial pressure on a steel die of desired shape and size. The load can be optimized by roughly measuring the green density of pellets using its physical dimensions and weight. A lubricant is applied to the surfaces of the moving parts of the die to prevent the powder from sticking. The addition of a few drops of binder (2% PVA solution in water) is often done with calcined powders before pressing pellets to ensure good densification.

Fig 2.2 A typical hydraulic press

2.2.3 High-Temperature Furnace

Various thermal exposures are required to synthesize and sinter ceramics, which are given by the high-temperature furnaces. Sintering of ceramic materials consolidates them at a high temperature below their melting point until the material of the separate particles diffuses to the neighbouring powder particles, giving the highest possible density. Densification is achieved by eliminating pores at the expense of free energy. Different heating elements, such as SiC rods or metallic resistive heating coils, are used depending on the desired high temperatures. The ramp rate of heating and dwelling time in furnaces can be regulated using a temperature controller. Ceramic insulation like Alumina, magnesia etc. are used for the walls and gates of the furnaces to ensure thermal insulation. A typical picture of the used muffle furnace is shown in Fig 2.3.

Fig 2.3 A typical high-temperature muffle furnace

2.2.4   X-Ray Diffractometer

X-ray diffraction (XRD) is the most essential analytical technique for studying crystal structural features such as symmetry, bond angle, bond lengths, atomic spacing, crystallite sizes, strain analysis, lattice characteristics, degree of crystallinity, quantitative phase analysis, etc. The principle of X-ray diffraction is based on the constructive interference satisfying Bragg's Law ($n\lambda = 2d_{(hkl)}\sin\theta$) for some particular angle of incidence as per the interplanar separation of the crystals. For characterizing powder samples, monochromatic X-rays (wavelength, λ) are diffracted from the atomic planes of spacing $d_{(hkl)}$ of a crystalline sample at the geometric angles (θ) of the detector, goniometer and X-ray generator assembly. The X−rays are generated by a cathode ray tube in the laboratory, while they are monochromatically filtered in synchrotron radiation emitted from the deaccelerating high-speed circulating electrons in storage ring injected from particle accelerators. The typical laboratory XRD and synchrotron XRD measurement set ups (at Indian beamline, Photon Factory, KEK, Tsukuba, Japan) for diffraction measurements are shown in Fig 2.4(b) and Fig 2.4(c), respectively. The radiation is collimated to concentrate and directed towards the sample. The diffracted

X−rays are then detected, processed, and counted. In a typical diffractogram, the intensities of the diffracted rays are plotted against their diffraction (2θ) angles, as shown the schematics of diffraction in Fig 2.4(a). All possible diffraction directions of the lattice are attained by scanning the sample through a 2θ range for a randomly oriented powder sample, whereas for the single-crystalline and thin-film samples, the assembly varies.

Fig 2.4 (a) Principle of Braggs' law for visualizing XRD, (b) Cu $K_{\alpha 1}$ based laboratory XRD Rigaku Miniflex and (c) Synchrotron XRD measurement station hutch

2.2.5   Scanning Electron Microscope

A scanning electron microscope (SEM) scans the surfaces of the sample with a concentrated stream of electrons, as shown in Fig 2.5(a). Electrons hitting the surface of the sample with a very narrow beam interact with atoms and produce micrographs having a large depth of field. This creates a characteristic three-dimensional image of the sample, which is useful for understanding its surface structure. Secondary electrons, backscattered electrons, characteristic X-rays, absorbed current (specimen current), transmitted electrons and other signals are collected, amplified, and detected using a scintillator-photomultiplier detector to obtained different characteristics of the sample. The gathered data are translated into electrical signals, and the scan is utilized to

produce a picture of the surface of materials. The electron dispersive spectroscopy (EDS) attachment in SEM offers the characterization of the materials through element analysis, and concentration detection. In it the characteristic x-rays are emitted from the sample due to bombardment of electrons over the material. Each element has a unique atomic structure, permitting a unique set of x-ray peaks on its electromagnetic emission spectrum, which also vary as its chemical state. An energy-dispersive spectrometer stimulates and measures these characteristic X-rays for reliable compositional analysis. A picture of a SEM instrument with various detectors is shown in Fig 2.5(b).
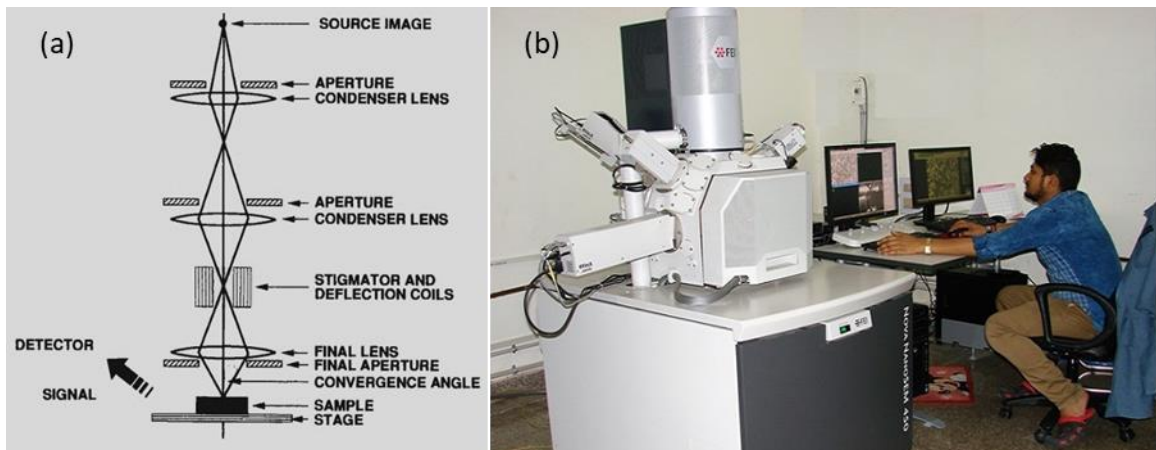

Fig 2.5 (a) Schematic of a SEM instrument and (b) A typical Zeiss SEM instrument

2.2.6 X-ray photoelectron spectroscopy

X-ray photoelectron spectroscopy (XPS) is a surface-sensitive quantitative technique based on the photoelectric effect and is useful for studying surface chemistry and bonding in materials. By photoionization, electrons are ejected onto the Al-anode to produce soft x-ray photons of usually 1486eV to irradiate the surface of the sample. A schematic of XPS and a picture of a real instrument are shown in Fig 2.6(a) and Fig 2.6 (b), respectively. The photons interact with sample atoms, and their chemical ionization

states are estimated from the measurement of the kinetic energy (E_K) and the number of ejected electrons from the sample. The original binding energy (E_B) experienced by an electron in the sample can be calculated using equation (2.1).

$$E_K = h\nu - E_B - \phi \tag{2.1}$$

Here, $h\nu$ is the energy of the incident photon and ϕ is the work function-like term that corrects the work function of the instrument because of the contact potential. Ultrahigh vacuum conditions are maintained within the spectrometer to limit electron scattering and surface contamination. Different atoms have different electron shells with unique E_B for various ionization states, which can be used to identify the elements. In an XPS spectrum, the number of emitted photoelectrons are plotted with their E_B to facilitate the identification of all the chemical states of the elements except H and He.
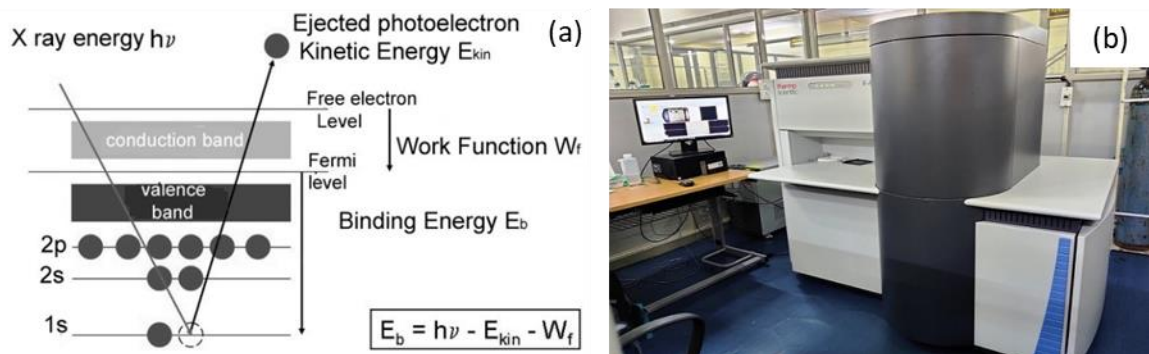

Fig 2.6 (a) Principle of XPS and (b) A typical Thermo Fisher Scientific XPS instrument

2.2.7 Impedance analyzer

Impedance analyzers are a class of instruments that measure highly accurate complex electrical impedance and various other parameters such as admittance, conductance, resistance, reactance, susceptance, inductance, capacitance, etc. The absolute, real and imaginary parts and the phase angles of these parameters are also

facilitated by this instrument. It involves frequency and temperature dependent measurement of a phase-sensitive current and voltage across the sample. Impedance spectroscopy is a universal and powerful tool to study soft matter and determine the frequency-dependent characterization of electronic components, electronic circuits and materials exhibiting dielectric behaviour. It provides essential information on the dielectric behaviour of materials giving dielectric permittivity (ε), dielectric loss (tanδ), electrical conductivity (σ), etc. A schematic of the temperature and frequency-dependent measurement setup using impedance analyzer is shown in Fig 2.7.
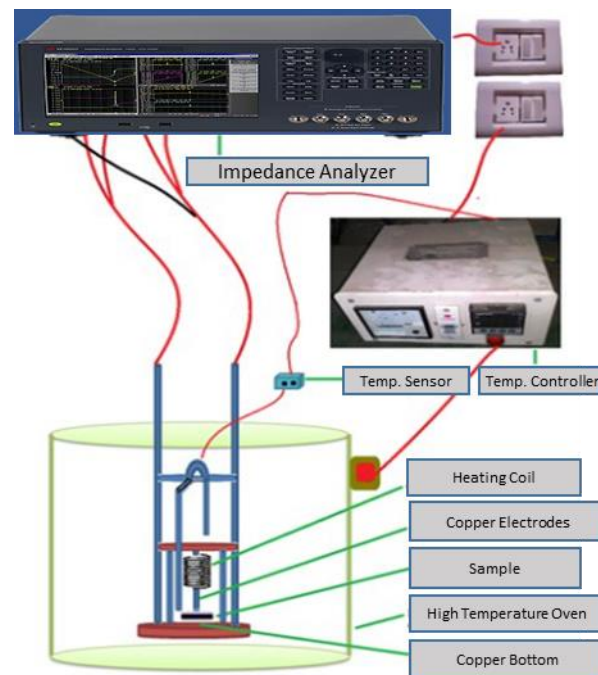

Fig 2.7 Schematic setup for temperature-dependent impedance spectroscopic measurements

2.2.8 d_{33} meter

d_{33} meter is used to measure the piezoelectric strain coefficients. In this measurement, the sample is clamped and subjected to a low-frequency force (~110Hz).

The frequency is kept below the resonance frequency of the test material. Poled ferroelectric ceramics and single-crystalline piezoelectric materials can develop charges on opposite surfaces after applying such a low-frequency force. The charges are then processed into signals and compared with a built-in reference to measure d_{ij} coefficients in charge per unit force, depending upon the sample measurement case. The most commonly used mode is "quasi-static" or "Berlincourt", measuring d_{33} in which applied force and measuring signal are both executed in the same direction of polarization. A d_{33} measuring instrument from piezotest, UK used in the present work is shown in Fig 2.8.

Fig 2.8 A typical d_{33} meter instrument

2.2.9 P-E loop tracer

P-E loop tracer works on the basic principle of the Sawyer tower circuit, as shown in Fig 2.9(a). The circuit consists of two capacitors arranged in series, one is the test dielectric sample and the other is a linear known-valued reference capacitor. The capacitance of the reference capacitor is kept much higher than the sample to maximize the voltage drop across the sample. The drive voltage in the circuit is almost equal to the voltage across the sample, and the voltage across the reference capacitor gives the

polarization of the sample. Voltages across these capacitors are given in the vertical and horizontal plates of the oscilloscope to measure the electric field across the sample. In an actual P-E setup, instead of measuring charges directly, the instantaneous current is measured and then integrated to evaluate charges. In Fig 2.9(b), a prototypical circuit is shown to measure the P-E loop, and Fig 2.9(c) depicts the Radiant, USA, Precision Premier II ferroelectric loop tracer, with a sample holder unit used in the present work.
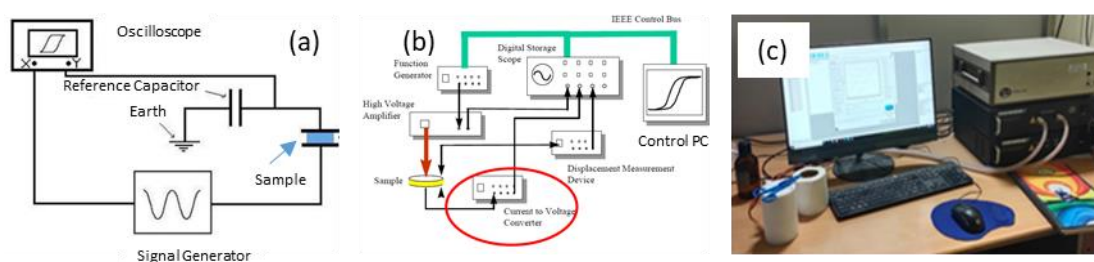

Fig 2.9 (a) Sawyer Tower circuit, (b) ferroelectric measurement setup and (c) Radiant Technology's Precision Premier P-E loop measurement setup

2.3 Synthesis of (1-x)Ba(Cu$_{1/3}$Nb$_{2/3}$)O$_3$-(x)PbTiO$_3$ Ceramics

The synthesis of all the compositions of solid solution has been done by the conventional solid-state ceramic route. The starting precursors used to synthesize the samples are high-purity analytical reagent (AR) grade from Sigma-Aldrich chemicals [BaCO$_3$ (99.9%), CuO (99%), Nb$_2$O$_5$ (99.99%), PbO (99%) and TiO$_2$ (99%)]. The raw compounds are weighted in the desired ratio for their stoichiometric composition and mixed for 10 minutes using a mortar and pestle before grinding in the ball mill. Six to twelve hours of high-energy milling was done in the presence of AR-grade ethanol as a mixing media. After mixing, the powder was dried and calcined in a muffle furnace in alumina crucibles.

2.3.1 Optimization of Calcination Conditions of (1-x)BCN-(x)PT Ceramics

In order to eliminate impurities and ensure pure perovskite phase formation, the calcination temperature and time were optimized for $x = 0$, 0.20, 0.59 and 0.75 compositions and then these synthesis parameters were used for the synthesis of other neighbouring compositions. The optimization of the calcination process was done by successive x-ray diffraction (XRD) pattern recordings as the synthesis temperature increases. In this process, the phase formation has been observed as the reduced intensity of the XRD peaks of the initial precursors and a simultaneous rise in the XRD peaks of the desired phase. The XRD patterns of the (0.41)BCN-(0.59)PT composition calcined for 5 hours at different temperatures are shown in Fig 2.10(a). Being an intermediate temperature in the optimization process, the XRD pattern of 700°C, shown in Fig 2.10(b), contains ~35% phase fraction of other multiple phases in addition to the final perovskite crystal structural peaks of pure (0.41)BCN-(0.59)PT, which constitute ~65% of it. These other phases are the unreacted oxides of initial precursors (TiO_2 and Nb_2O_5) and the intermediate impurity phases ($Pb_2Nb_2O_7$, $Ba_{2.5}Nb_{1.5}CuO_{7.5}$ and $BaCu_3O_4$). The XRD peaks corresponding to these phases are marked in Fig 2.10(b). It can be seen from Fig 2.10(a) that a pure perovskite phase free from any impurities is obtained for the sample calcined at 900°C. Similarly, XRD patterns of the samples for the optimization process of the $x = 0.20$ and 0.75 compositions are shown in Fig 2.10(c and d), respectively. The optimum calcination temperature for the $x = 0.20$ composition is 950°C, while the same is 975°C for the composition with $x = 0.75$, as the tiny extra peaks of little impurities can be taken care of, while sintering. After proper optimization, the composition ranges, $0.20 \leq x \leq 0.40$ and $0.70 \leq x \leq 0.85$, were synthesised in a similar fashion as the compositions 0.20 and 0.75, respectively. The rest of the compositions were synthesized with the conditions as that for the (0.41)BCN-

(0.59)PT composition. The calcination time was fixed at 5 hours for all the compositions except for BCN, which was obtained in pure phase after 10-hour calcination at 900°C of 12-hour ball-milled precursor.
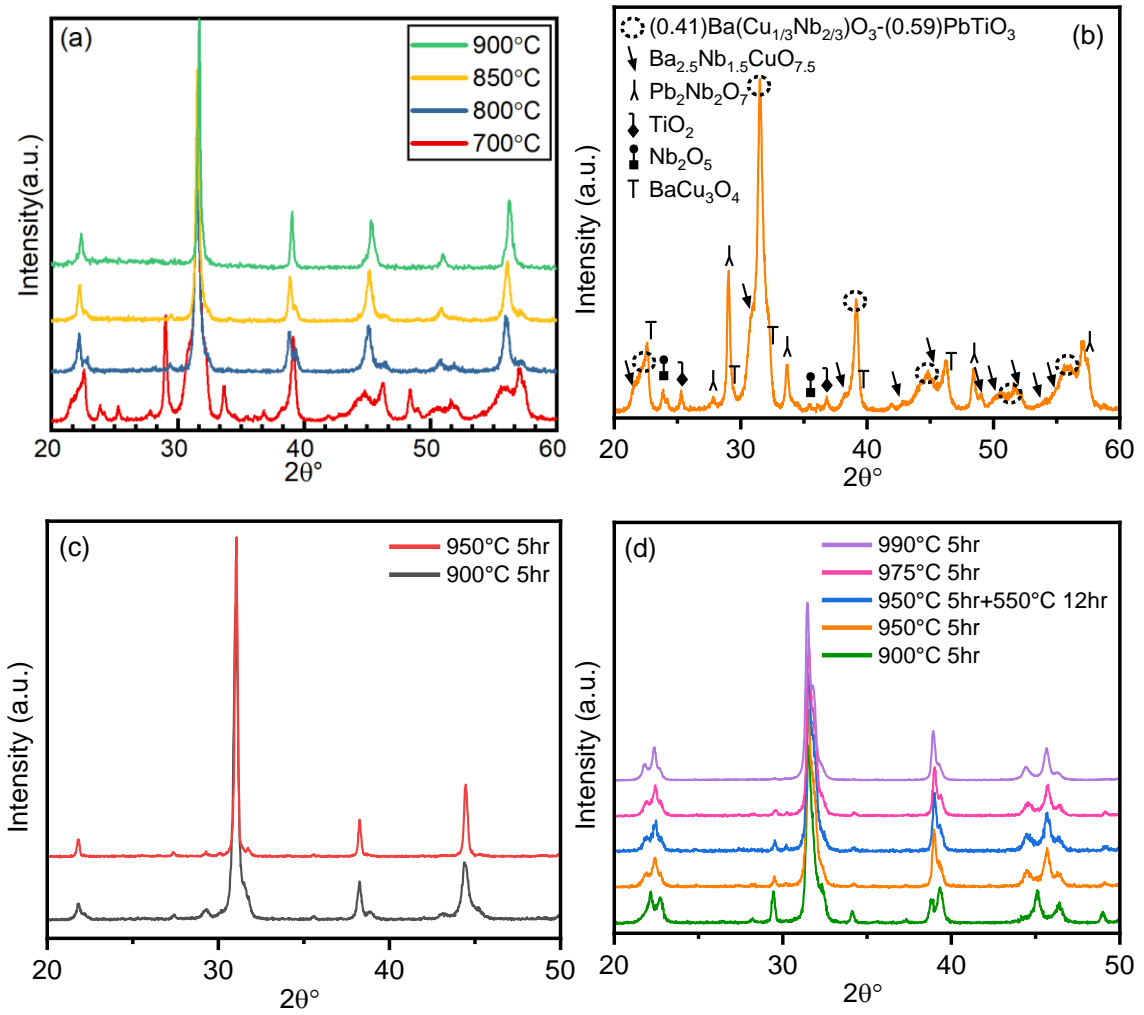

Fig 2.10 XRD patterns for illustration of optimization of calcination temperature (a) x = 0.59, (c) 0.20 and (d) 0.75 composition of (1-x)BCN-(x)PT ceramic calcined at various temperatures; (b) XRD pattern of 0.59 composition calcined at 700°C showing the secondary phases present in the material

2.3.2 Optimization of Sintering Conditions for Bulk Characterization of (1-x)BCN-(x)PT Ceramics

For cold compaction of powders into disc pellets, a few drops of binder (2% PVA solution in water) were added to the calcined powder and pressed into circular disk form by applying a 12-ton load to the powder in a cylindrical die using a uniaxial hydraulic press. The removal of the binder was done by heating the green pellets at 550°C for 15 hours. To avoid significant volatilization of Lead during sintering, a small amount of calcined powder was placed along with the pellets and sealed under inverted Alumina crucible by fired MgO powder to maintain a closed sintering atmosphere. The sintering temperature and dwell time are optimized to 1050°C and 2-hours, respectively. The bulk density of the ceramics was measured by the Archimedes method. All the samples in the composition region $0.20 \leq x \leq 0.70$ had a high density ($\geq$99%). The density after the 0.70 composition decreases with increasing PT concentration by 97% to 93% in the composition region $0.75 \leq x \leq 0.95$. A higher sintering temperature (1120°C) for the ceramics of this compositional region increases the density, but simultaneous melting of the material may follow, posing questions on compositional homogeneity and concentration.

2.4 Instrumental Specification

A Retsch PM400 MA high-energy ball mill has been used to mix reactant powder. XRD patterns have been recorded at Rigaku Miniflex and a 9kW Cu-based rotating anode SmartLab Rigaku diffractometers. The synchrotron Indian beamline at Photon Factory, KEK, Japan, with wavelengths 1.235Å and 1.2266Å was also used to characterize the samples. To record powder X-ray diffraction patterns, sintered pellets were crushed into fine powders and annealed at 550°C for 15 hours. For dielectric and

polarization-electric field (P-E) hysteresis measurements, pellets have been processed for surface polishing and cleaning, followed by painting fired on electrodes on either side with silver conducting paste. The poling of electroded pellets were done at 50°C in a silicon oil bath by applying a DC bias voltage slightly below the individual breakdown strengths of the samples for various compositions. Dielectric measurements have been done with the Keysight Impedance Analyzer (E4990A). The P-E hysteresis measurements have been performed on Radiant Technology's Precision Premier-II ferroelectric loop tracer in a silicon oil bath at 50Hz signal. Scanning electron microscopy (SEM) and energy dispersive spectroscopy (EDS) measurements have been done for microstructural and elemental characterization using Zeiss EVO-SEM. X-ray photoelectron spectroscopic measurements have been recorded by Thermo Fisher Scientific XPS.

2.5   Rietveld Structure Refinement Method for Crystal Structure Refinement

2.5.1   Introduction

For the identification and confirmation of crystal structures and phase analysis of materials, Rietveld Refinement is the most precise tool commonly used in the field of material science that refines parameters in models for crystal structures. It is widely used for interpreting X-ray and neutron diffraction data of polycrystalline samples. As clear from the name, the first ever computer-based analytic procedures were done by H. M. Rietveld, and he freely and widely shared his computer program along with two papers, Rietveld (1967) and Rietveld (1969) [70,71]. For the refinement of the crystal structure of polycrystalline materials, its powder XRD pattern is generated using theoretical calculation in the software, such as FullProf Suite, GSAS, TOPAS, MAUD

etc., in which they are compared with the observed XRD pattern and simultaneously refined. In this thesis, the crystal structures are refined using FullProf Suite using the least square method.

The diffraction data contains intensity at many points (y_i) at each of several thousand equal steps (i), each contributed by many Bragg reflections. The theoretical intensity (y_{ci}) in software, on the other hand, is calculated from the structure factor and other background intensities. In equation (2.2), various contributions of the calculated intensities are given.

$$y_{ci} = s \sum_{i=1}^{n} L_K * m * |F_K|^2 * \varphi(2\theta_i - 2\theta_k) * P_K * A + y_{bi} \tag{2.2}$$

$$F_K = \sum_{j}^{n} N_j f_j e^{2\pi i[(hx_j + ky_j + lz_j)]} e^{-M_j} \tag{2.3}$$

Here, s is the scale factor, K represents the Miller indices, h k l, for a Bragg reflection, L_K contains the Lorentz polarization, m is the multiplicity factor, F_K is the structure factor for the Kth Bragg reflection defined in equation (2.3), φ is the reflection profile function used for specimen and instrument specific features, P_K is the preferred orientation function which takes care of systematic distortions of the reflection intensities, *A* is an absorption factor and y_{bi} is the background intensity at the ith step which is obtained from either a background function, an user given background intensities, or using linear interpolation between user-selected points in the pattern. In equation (2.3) the x_j, y_j and z_j are position parameters of jth atom in unit cell, N_j is site occupancy multiplier, and M_j is thermal parameter. The least squares minimization procedures lead to a set of normal equations involving derivatives of all of the calculated intensities with respect to each adjustable parameter. These are soluble by inversion of the normal matrix with elements (M_{jk}) given by equation (2.4).

$$M_{jk} = -\sum_{i}^{n} 2w_i \left[(y_i - y_{ci}) \frac{\partial^2 y_{ci}}{\partial x_j \, \partial x_k} - \left(\frac{\partial y_{ci}}{\partial x_j} \right) \left(\frac{\partial y_{ci}}{\partial x_k} \right) \right] \tag{2.4}$$

The 'best-fit' desired is the best least-squares fit to all of the thousands of y_i's simultaneously. The quantity minimized in the least-squares refinement is the residual, S_y, is given by equation (2.5)

$$S_y = \sum_{i}^{n} w_i \left[(y_i - y_{ci})^2 \right] \tag{2.5}$$

Here, w_i is the inverse of y_i. To estimate the diffraction profiles via Rietveld method, various kind of functions have been defined in the program. An extensively used profile shape fitting function is Pseudo-Voigt function which is a linear combination of Lorentzian and Gaussian peak functions defined as equation (2.6). The width of diffraction peaks, also known as full width at half maximum (FWHM), defined as equation (2.7).

$$pV(x) = \eta L(x) + (1 - \eta) G(x) \tag{2.6}$$

$$FWHM = U * tan^2(\theta) + V * \tan(\theta) + W \tag{2.7}$$

Where, U, V and W are the refinable parameters and are different for different diffractometer while fixed for a particular diffractometer, if the effect of line broadening does not contribute to the diffraction data. For each phase present the parameters that can be simultaneously refinable are scale factor, specimen-profile breadth parameters (U, V and W), lattice parameters, Overall temperature factor, Individual anisotropic thermal parameters, Preferred orientation, Crystallite size and microstrain. For refining globally, the following parameters are considered simultaneously, 2θ-Zero, instrumental profile, profile asymmetry, background, wavelength, specimen displacement, specimen transparency absorption.

Rietveld Refinement process adjusts the refinable parameters until the residual is minimized to give the 'best fit' of the entire calculated pattern to the entire observed pattern. The 'best fit' however, depend on the adequacy of the model and on whether a global minimum is achieved rather than a local or false minima. The structural parameters obtained from refined structure giving the satisfactory fit are accepted as the correct crystal structure. Different agreement factors are taken to justify the quality of fits between observed and Rietveld calculated diffraction profiles quantitatively. The weighted profile R-factor, denoted by R_{wp}, is very significant among other R-factor as it minimizes the residual in numerator. It is the square root of the ratio of χ^2 to the weighted intensities [Young (1993)]; is given by equation (2.8). The expected R parameter, R_{exp} defined as equation (2.9). Another important and popular criterion of judging the fit is goodness of fit, 'S' which is square root of χ. The relation among these is defined as equation (2.10). Another criterion of judgement the quality of fit is R-pattern, Rp, which is defined as equation (2.11).

$$R_{wp} = \left[\frac{\sum w_i \left[(y_i - y_{ci})^2 \right]}{\sum w_i (y_i)^2} \right]^{1/2} \tag{2.8}$$

$$R_{exp} = \left[\frac{N}{\sum w_i (y_i)^2} \right]^{1/2} \tag{2.9}$$

$$\chi^2 = S^2 = \frac{R_{wp}}{R_{exp}} \tag{2.10}$$

$$R_p = \frac{\sum |(y_i - y_{ci})|}{\sum y_i} \tag{2.11}$$

Where, N, stands for the number of data points. For any Rietveld fitting, χ^2 should not decrease below unity. Values of χ around 1.7 also indicates dome problem in the physical relevance of the refined parameters. The cases happens when the fitting of the data is performed by overestimating the standard uncertainties or including extra parameters in the refinement and the structural model is incorrect. In such cases Rietveld program is forced to fit the noise which in turn reduces the value of χ^2 less than

1. Moreover, if χ^2 comes very close to 1, it does not essentially imply that the considered model or corresponding fit is correct. Different structural models can result into similar fitting due to inadequate or poor diffraction data.

2.5.2 Details of the Rietveld Refinement

For crystal structural analysis, full pattern profile refinement of diffraction data recorded from Cu anode-based HR-XRD in the 2θ range $20°$-$120°$ and from synchrotron XRD in the 2θ range $15°$-$80°$. These XRD patterns have been analyzed using the Rietveld Method employing FullProf Suite software [72]. In Rietveld Refinement, the background has been fitted by taking linear interpolation between refinable heights. The pseudo-voigt functions was used to fit the XRD peak shapes. Variations of several parameters, such as zero correction, background points, lattice parameters, profile width parameters with instrument profile consideration, peak function, anisotropic broadening, atomic coordinates, and thermal parameters, are employed to fit the experimental XRD patterns. The solid solution has a perovskite-type structure and shares the A-site between Ba/Pb and the B-site among Cu/Nb/Ti ions. The *Pm-3m* space group is used for the cubic phase, with A-site fixed at Wyckoff positions 1(a) (0,0,0), B-site at 1(b) (½,½,½) and oxygen ions at 3(c) (½,½,0). In the tetragonal structure with a *P4mm* space group, A-site was fixed at Wyckoff positions 1(a) (0,0,0), B-site and O_I at 1(b) (½,½,z) and O_{II} oxygen ions at 2(c) (½,0,z). In the monoclinic *Pm* space group, Wyckoff positions were 1(a) (x,0,z) for A-site and O_I atoms, and 1(b) (x,½,z) for B-site atoms, O_{II} and O_{III}.